A model for internal oscillations in geysers, with application to Old Faithful (Yellowstone, USA)

Maxwell L. Rudolph[1,*] **Robert A. Sohn**[2]

[1]*Portland State University, Geology, PO BOX 751, Portland OR 97201*

[*]*Address correspondence to* maxwell.rudolph@pdx.edu

[2]*Woods Hole Oceanographic Institution, Geology and Geophysics, 360 Woods Hole Rd., Woods Hole, MA, 02543*

ABSTRACT

We present a mechanical model for internal oscillations in geysers with "bubble trap" configurations, where ascending gas or vapor becomes trapped beneath the roof of a cavity that is laterally offset from the eruption conduit. We consider two cases, one in which the trapped gas behaves as an isothermal ideal gas, and one where it is treated as isenthalpic steam. In both cases the system behaves as a damped, harmonic oscillator with a resonant frequency that is sensitive to the conduit geometries and fluid volumes. We use the model to predict internal oscillation frequencies for Old Faithful geyser, in Yellowstone, USA, using conduit geometry constraints from the literature, and find that the frequencies predicted by the model are consistent with observations (~1 Hz). We show that systematic frequency increases during the recharge cycle, when the fluid volume of the system is increasing due to recharge, are consistent with either a decrease in the amount (both volume and mass) of trapped gas or vapor, a decrease in the eruption conduit area, or a combination of both.

1. INTRODUCTION

Geysers have intrigued scientists for centuries (e.g., Mackenzie, 1811; Bunsen, 1847), but despite this long history of research, some aspects of their internal dynamics remain poorly understood. While it is clear that geysers erupt by converting thermal energy into mechanical energy via vapor generation in response to depressurization (e.g., Kieffer, 1977; Steinberg et al., 1981), geysers also display dynamic behaviors during quiescent periods between eruptions, where the fluid pressure in the eruption conduit oscillates at characteristic frequencies (Birch and Kennedy, 1972; Hutchinson et al., 1997; Kedar et al., 1998; Karlstrom et al., 2013; Munoz-Saez et al., 2015). Internal oscillations in geysers could be produced by resonant excitation of fluid in the conduit, by the passage of bubbles, or by oscillatory motion of all fluids filling the conduit, the case considered in detail here.

Most extant geyser models have conceptualized the conduit system as one or more vertical pipes/chambers (e.g., Steinberg et al., 1981; Dowden et al., 1991; Ingebritsen and Rojstaczer, 1993; Kagami, 2010; Anatolyevich, 2013; O'Hara and Esawi, 2013; Namiki et al., 2014; Munoz-Saez et al., 2015; Alexandrov et al., 2016), but geophysical and videographic data from several geysers has recently provided evidence for the existence of a laterally offset cavity, referred to henceforth as a 'bubble trap' (Belousov et al. 2013) that is connected to a vertical eruption conduit by a horizontal feeder (e.g., Cros et al., 2011; Belousov et al., 2013; Vandemeulebrouck et al., 2013; Vandemeulebrouck et al., 2014). In a system with this geometry, (Figure 1) ascending non-condensable gas or superheated vapor cannot escape the bubble trap unless the total gas volume exceeds some threshold (e.g., Belousov et al., 2013; Adelstein et al. 2014). As a consequence, fluid in the eruption conduit loads a compressible volume of trapped gas, and the response of this coupled system to perturbations provides a plausible explanation for the pressure oscillations observed during recharge (e.g., Vandemeulebrouck et al., 2014). Previous efforts have modeled the dynamic behavior of a liquid column overlying a gas bubble in a vertical conduit (e.g., Dowden et al., 1991; Kagami, 2010; Alexandrov et al., 2016), but a complete mechanical model for oscillations within geysers with a bubble trap has not been developed.

We generate an equation for fluid motion by considering the force balance across the gas-liquid interface in an idealized geyser system with a bubble trap offset from the conduit. We consider two different scenarios for the thermodynamic behavior of the gas volume in response to a pressure perturbation: 1) the volume behaves as an isothermal ideal gas, and 2) the volume behaves as isenthalpic steam. We show that in both cases the system behaves as a damped, harmonic oscillator with a resonant frequency that depends on the conduit geometry and the volumes of gas and liquid in the conduit system. The ideal gas and steam assumptions yield similar results for the parameter space we explored, and we develop an analytical formula for the resonant frequency that closely matches our modeling results. We apply the model to pressure data recorded in the eruption conduit of Old Faithful geyser in Yellowstone National Park, USA (Kedar et al., 1998), and find that we can reproduce the oscillation frequencies observed during the geyser's recharge phase using parameters that are consistent with videographic (Hutchinson et al., 1997) and geophysical (Vandemeulebrouck et al., 2013) constraints of the subsurface conduit geometry.

2. DYNAMIC MODEL OF A GENERALIZED BUBBLE TRAP CONFIGURATION

In its simplest form a bubble trap configuration includes a reservoir connected to a conduit (Figure 2). The connection between the conduit and the reservoir is some distance (*H*) beneath the roof of the bubble trap, and as a result, any gas entering the system either condenses or is trapped. The gas-liquid interface is located some distance (z_1) above the horizontal connector, such that when $z_1 = H$ the bubble trap is completely full of liquid, and when $z_1 = 0$ it is completely full of gas. The total liquid volume is given by $V_l = S_b z_1 + S_c z_2$, where z_2 is the liquid level in the eruption conduit, and S_b and S_c are the cross-sectional areas of the bubble trap and eruption conduit, respectively. The gas volume is given by $V_g = S_b(H\text{-}z_1)$.

To develop an equation of motion for the gas-liquid system we assume that the liquid mass and volume are constant, such that $\partial V_l/\partial t = 0$, yielding:

$$z_2 = C - S_r z_1 , \quad \text{(1a)} \quad z_2 = C - S_r z_1$$

$$\dot{z}_2 = -S_r \dot{z}_1 , \quad \text{(1b)} \quad \dot{z}_2 = -S_r \dot{z}_1$$

$$\ddot{z}_2 = -S_r \ddot{z}_1 . \quad \text{(1c)} \quad \ddot{z}_2 = -S_r \ddot{z}_1$$

where $S_r = S_b/S_c$, and $C = V_l/S_c$. A force balance across the gas-liquid interface yields

$$p_g S_b = -F_i + F_h + F_f + F_s \tag{2}$$

, where p_g is the gas pressure, F_i is the inertial force exerted by the liquid mass on the gas, F_h is the hydrostatic load on the gas, F_f is viscous drag from wall friction, and F_s is surface tension.

We can apply Newton's second law for a variable mass system (because liquid mass moves between the conduit and the reservoir) to derive an expression for the inertial force (F_i):

$$F_i = \rho S_b \frac{\partial}{\partial t}\left(z_1 \frac{\partial z_1}{\partial t}\right) - \rho S_c \frac{\partial}{\partial t}\left(z_2 \frac{\partial z_2}{\partial t}\right) = \rho S_b \left(\left(1 - S_r\right)\dot{z}_1^2 + \left(C + \left(1 - S_r\right) z_1\right)\ddot{z}_1\right), \tag{3}$$

$$F_i = \rho S_b \frac{\partial}{\partial t}\left(z_1 \frac{\partial z_1}{\partial t}\right) - \rho S_c \frac{\partial}{\partial t}\left(z_2 \frac{\partial z_2}{\partial t}\right) = \rho S_b\left((1 - S_r)\dot{z}_1^2 + (C + (1 - S_r) z_1)\ddot{z}_1\right)$$

where ρ is liquid density. The hydrostatic load on the gas (F_h) is determined by the difference between the liquid level in the bubble trap and eruption conduit, and is given by:

$$F_h = S_b\left(p_0 + \rho g (z_2 - z_1)\right) = S_b(p_0 + \rho g (C - (S_r + 1)) z_1), \tag{4}$$

where p_0 is atmospheric pressure and g is gravitational acceleration.

Friction in pipe flow is proportional to the pipe dimensions, the roughness of the pipe walls, and the flow velocity, and acts in the direction opposite to the flow. Here we assume that the friction term is controlled by conditions in the eruption conduit because in natural systems it is expected to be taller and narrower than the bubble trap, and thus has a higher surface area per unit volume with correspondingly higher flow velocities (Eq. 1). Neglecting friction in the bubble trap, we can use the Darcy-Weisbach equation to express the friction force associated with flow in the eruption conduit as:

$$F_f = \mathrm{sgn}\left(\dot{z}_2\right)\frac{1}{4}\sqrt{\frac{\pi}{S_c}}f_D\rho S_b z_2 \dot{z}_2^2 = -\mathrm{sgn}\left(\dot{z}_1\right)\frac{1}{4}\sqrt{\frac{\pi}{S_c}}f_D\rho S_b S_r^2\left(C - S_r z_1\right)\dot{z}_1^2\,, \qquad (5)$$

$$F_f = \mathrm{sgn}(\dot{z}_2)\frac{1}{4}\sqrt{\frac{\pi}{S_c}}f_D\rho S_b z_2 \dot{z}_2^2 = -\mathrm{sgn}(\dot{z}_1)\frac{1}{4}\sqrt{\frac{\pi}{S_c}}f_D\rho S_b S_r^2(C - S_r z_1)\dot{z}_1^2$$

where f_D is the Darcy friction factor. We note that the Darcy-Weisbach equation assumes steady unidirectional flow, and that more complete treatments of oscillatory pipe flows exist (e.g. Pedocchi and Garcia, 2009). However, we adopt it here for simplicity and explore values of the friction factor that encompass the range that would be representative of oscillatory flows.

If the surface area, S_b, of the bubble trap is large enough, then the gas-liquid interface is approximately planar and surface tension can be ignored (i.e., $F_s = 0$). We can substitute Equations (2-4) into the force balance to derive an equation of motion for the gas-liquid interface in the bubble trap:

$$\left(C + \left(1 - S_r\right)z_1\right)\ddot{z}_1 = \frac{p_0 - p_g}{\rho} + gC - g\left(S_r + 1\right)z_1 - \left(1 - S_r\right)\dot{z}_1^2 - \mathrm{sgn}\left(\dot{z}_1\right)\frac{1}{4}\sqrt{\frac{\pi}{S_c}}f_D S_r^2\left(C - S_r z_1\right)\dot{z}_1^2\,. \quad (6)$$

$$(C + (1 - S_r)z_1)\ddot{z}_1 = \frac{p_0 - p_g}{\rho} + gC - g(S_r + 1)z_1 - (1 - S_r)\dot{z}_1^2 - \mathrm{sgn}(\dot{z}_1)\frac{1}{4}\sqrt{\frac{\pi}{S_c}}f_D S_r^2(C - S_r z_1)\dot{z}_1^2$$

The response of the gas pressure to a change in z_1 depends on the thermodynamic behavior of the two-phase system, which determines the relationship between p_g in Equation 6, gas volume and mass, and temperature. We consider two cases. First, a bubble trap filled with an ideal gas, and second, a bubble trap filled with water vapor (steam). Both cases may be relevant to natural systems in that some geyser fluids may contain both non-condensable gases and water vapor (e.g. Hurwitz et al. 2016)

2.1 The Ideal Gas Model

For simplicity, we assume isothermal conditions in our analysis and treat the gas volume as an Ideal Gas (e.g., Kagami, 2010):

$$\frac{p_g V_g}{n} = RT \,, \qquad (7) \qquad \frac{p_g V_g}{n} = RT$$

where n is the number of moles of gas, R is the gas constant, and T is the gas temperature. This approach neglects any heat and mass transfer between liquid and vapor phases, as well as heat transfer with the conduit walls, but these processes occur over time-scales that are long relative to the propagation time of pressure pulses in the conduit system, so we ignore them for the purpose of studying the instantaneous system response to small perturbations.

This non-linear equation of motion can be solved numerically to show that under physically plausible parameterizations the system behaves as a damped, harmonic oscillator (Figure 3). To relate the resonant frequency to the model parameters we use an approximate solution to the equation of motion (Eq. 6) formulated by considering small oscillations about an equilibrium state. Consider solutions of the form:

$$z_1(t) = \bar{z} + \hat{z}, \qquad (8)$$

where $\bar{z}$ is an equilibrium solution to Eq. 6 and $\hat{z}(t)$ is an oscillatory perturbation of the form $Ae^{i\omega t}$ where the amplitude $A << \bar{z}$. Differentiating Eq. (6) with respect to t, we obtain:

$$C\dddot{z} + (1 - S_r)(\dot{z}\ddot{z} + z\dddot{z}) = \frac{-\dot{p}_g}{\rho} - g(S_r + 1)\dot{z} - 2(1 - S_r)\dot{z}\ddot{z}. \tag{9}$$

We introduce an effective bulk modulus K for the bubble trap. Here, this is the isothermal bulk modulus for an ideal gas. We can re-write the pressure time derivative in Eq. 9 as $\dot{p}_g = K\frac{i\omega\hat{z}}{H-\bar{z}}$. Substituting Eq. 9 and its derivatives, and cancelling terms, we obtain:

$$\omega^2(C\hat{z} + (1 - S_r)(\hat{z}^2 + (\bar{z}\hat{z} + \hat{z}^2))) = \frac{K}{\rho}\frac{\hat{z}}{H-\bar{z}} + g(S_r + 1)\hat{z} - 2(1 - S_r)\hat{z}^2 \tag{10}$$

We drop all terms of order O($\hat{z}^2$) and obtain an expression for the resonant frequency:

$$\omega = \left[\frac{-\frac{K}{\rho}\frac{1}{\bar{z}-H} + g(S_r+1)}{C + (1-S_r)\bar{z}}\right]^{1/2}, \tag{11}$$

that closely approximates the oscillation frequency obtained from our numerical experiments (Figure 3b, S1-4).

2.2 Steam Model

For the steam-filled bubble trap, we use the IAPWS IF-97 steam tables (Wagner et al. 2000) implemented in the ***XSteam*** software package (xsteam.sourceforge.net), assuming isenthalpic conditions in the bubble trap. The steam tables provide an equation of state for vapor pressure $p_g(h,V)$, where h is enthalpy per unit mass, and $V=S_b\,(H-x_1)$ is the vapor volume. We first determine the initial condition by specifying values $z_{1,0} = z_1(0)$ and $dz_0 = z_2(0) - z_1(0)$ (the difference in liquid fill level between the conduit and bubble trap). The initial values allow us to determine the initial vapor volume, total liquid volume, and the initial vapor pressure $p_g(0)$. We then obtain the saturation specific enthalpy $h_{sat,0}$ for the initial vapor pressure and volume using the steam tables. Given the initial volume, specific volume, and specific enthalpy, we can calculate density, and hence vapor mass. We integrate Equation 6 numerically from these initial conditions, using the steam tables to calculate vapor pressure at constant specific enthalpy

$h=h_{sat,0}$. For small oscillations, we can again predict the frequency of oscillations using equation (11), substituting an isenthalpic bulk modulus K_h (calculated numerically). We show the approximate result based on Equation 11 together with a numerical solution in Figure 4 and Figures S5-9, demonstrating excellent agreement.

3. RESULTS

To explore the model behavior, we adopt a reference set of parameters representative of Old Faithful Geyser (OFG) in Yellowstone National Park, USA (Table 2). We performed a suite of calculations in which the bubble trap liquid level (z_1) is perturbed away from equilibrium by an amount F_a, and then allowed to oscillate freely. In the natural systems, this perturbation could be the injection of vapor or gas into the bubble trap from a deeper part of the system, or could be associated with conduit processes such as bubble ascent, expansion, and collapse, that perturb the pressure boundary condition at the gas-liquid interface in the bubble trap. Viscous resistance causes the system to behave as a stable, damped oscillator. Thus for sufficiently long periods of integration the system will always return to its static equilibrium position. We systematically varied each of the parameters independently to assess their effect on the oscillation frequency and the system phase space trajectory. We first discuss results for the isothermal ideal gas (IG) model and then consider the isenthalpic steam (S) model. In sections S1-S2, we also provide a non-dimensional form of the governing equations and discuss the sensitivity in terms of the dimensionless parameters.

A representative example of the behavior of the IG model for different values of the conduit area S_c is shown in Figure 3 and Figures S1-4. Of the parameters, we find that the initial position of the vapor-liquid interface $z_{1,0}$ and the conduit area S_c most significantly affect the oscillation frequency for small perturbations about the reference state, whereas F_a (perturbation amplitude) and f_D (friction coefficient) do not. The initial position of the interface determines the vapor/gas volume in the bubble trap and therefore the relative volume change associated with a unit change in the interface position. Increasing $z_{1,0}$ decreases the bubble trap vapor/gas volume, increasing the stiffness of the system and thus the oscillation frequency. In principle, the amplitude of the perturbation can affect the period of oscillations due to the non-linearity of the equation of motion, but this effect is not observed for reasonable choices of the damping coefficient, f_D (Figure S1). In general, resonant frequency increases with increasing $z_{1,0}$ and decreasing S_c.

The behavior of the steam model is shown in Figure 4 and Figures S5-9. We again explored the sensitivity of the resonant frequency to each of the control parameters, perturbed about the reference state given in Table 2. The steam model is sensitive to the same parameters (i.e., S_c and $z_{1,0}$) in the same way as the Ideal Gas model. As with the Ideal Gas model, the steam model's resonant frequency is essentially insensitive to the amplitude of the perturbation (Figure S5) and the choice of friction coefficient (Figure S9).

4. DISCUSSION

We have developed a mechanical model for the internal oscillations in a geyser with a bubble trap. We find that for plausible parameter choices the system behaves as a stable, damped oscillator, and that the oscillation frequency depends on the conduit geometry and the amount of liquid and gas in the conduit system. If the conduit and bubble trap geometry of a particular system can be constrained, then the model could be used to estimate the total fluid volume and the relative fractions of liquid and gas when the system oscillates in-between eruptions.

For the Ideal Gas model, we assumed isothermal conditions in order to permit a simple treatment of gas compressibility and addition of mass to the system, similar to the formulation of Kagami (2010). However, the oscillation frequency predicted by our model depends on the compressibility of the gas filling the bubble trap, and the compressibility of steam can differ from that of an isothermal ideal gas by an order of magnitude at equal temperature and pressure conditions, owing to condensation and vaporization during (de-)compression (e.g. Kieffer 1977, Grant and Sorey, 1979). Since water vapor is likely to be the dominant gas phase in most natural geyser systems (e.g., Hurwitz and Manga, 2016, and references therein), our steam model is preferred over the IG model although it is more complicated owing to the necessity of using steam tables, rather than an analytic formula, to calculate the gas properties.

To test the applicability of our steam model to natural systems we use it to compare model predictions with the pressure data acquired in OFG's eruption conduit by Kedar et al. (1998). These data were collected over a 30-minute time interval in October 1994 during the geyser's recharge phase, starting when the water level was ~15 m below the surface. We adopt a reference set of parameters (Table 2) based on best estimates from Hutchinson et al., 1997 and Vandemuelebrouck et al., 2013. When the water level in the conduit (z_2) is 10 m (~12 m below the ground surface), the conduit cross-sectional area, S_c, is greater than 4 m^2 (Hutchinson et al., 1997) and the oscillation frequency is ~0.7 Hz. The oscillation frequency then steadily increases to ~1 Hz (Figure 5B) as the water level in the conduit (z_2) rises 3 m and the conduit cross-sectional area decreases. Figure 7 shows the dependence of oscillation frequency on S_c and position of the vapor-liquid interface (z_1) with contours indicating the combinations of these parameters that yield resonant frequencies of 0.7 and 1.0 Hz. We find that our model reproduces the observed oscillation frequencies for the reference set of parameters, and that the systematic frequency increase during recharge could result from either a decrease in the vapor volume (an increase in z_1) or a decrease in the conduit cross-sectional area S_c. We address each possibility in turn.

During the recharge period leading up to an eruption, the vapor occupying the bubble trap must be in thermodynamic equilibrium with the immediately underlying liquid water. As additional fluid is added to the system, the conduit liquid level increases, increasing hydrostatic pressure in the bubble trap. Some condensation occurs to heat the underlying liquid and maintain equilibrium as the saturation temperature increases with increasing pressure. The amount of vapor condensation required to maintain equilibrium when fluid is added to the system depends on the thermal state of the system and the conduit dimensions (the larger the liquid-gas interface, i.e., S_b, the more condensation required for a given pressure increase). We performed calculations using the steam model in which fluid mass is added to the system (Figure 6). The enthalpy of the added fluid was chosen such that it was much higher than the saturation enthalpy at the initial temperature and pressure of the bubble trap. As high-enthalpy fluid is added, we calculate self-consistently the new temperature of the fluid in the bubble trap (steam, which in this case may include condensed water) and the liquid in the geyser system. As high-enthalpy fluid is added to the system, the bubble trap vapor volume increases, and the oscillation frequency decreases slightly, opposite to the observed trend.

Down-hole observations of the conduit of OFG (Hutchinson et al., 1997), reveal that S_c decreases by a factor of about two over the height interval from 10 m to 13 m considered in our analysis. This decrease in S_c can explain the observed increase in the oscillation frequency even if the vapor volume increases (Figure 7). Thus, if the geyser is recharged with high-enthalpy vapor, the internal oscillation frequency increase observed during the recharge period is consistent with the observed change in the conduit area. Conversely, if the geyser is recharged with near-saturation enthalpy steam then significant amounts of condensation may occur as the hydrostatic load on the vapor increases during recharge, and the vapor volume may decrease, with a commensurate increase in z_1. This scenario could also explain the observed increase in the oscillation frequency during recharge (Figure 7). Lacking constraints on the thermal state of the recharge fluid we cannot formally distinguish between the possibility that the frequency increases as a result of a decrease in the conduit area vs. a decrease in vapor volume, or some combination of the two. However, the videographic data of Hutchinson et al., (1997) clearly shows that S_c decreases significantly over the conduit interval in question, suggesting that the conduit area may exert a primary control on the oscillation frequency. In-situ pressure and temperature measurements in the eruption conduit of a geyser in El Tatio, Chile suggest that fluids in a geyser conduit are cooler than the saturation temperature immediately following an eruption and gain enthalpy during the recharge phase (Muñoz-Saez et al. 2015). Thus, it is likely that fluid added to the system during the recharge phase has higher-than saturation enthalpy, and significant condensation of vapor is unlikely to be caused by fluid addition.

While we enforce thermodynamic equilibrium between the liquid and vapor in the bubble trap when mass is added to the system, we do not account for disequilibrium heat/mass transfer between the vapor and liquid phases. We thus assume that the bubble trap vapor undergoes isenthalpic expansion and contraction on the timescale of internal oscillations, which is short relative to the timescale of disequilibrium heat/mass transfer. The latter timescale depends on the kinetics of mass transfer across the vapor-liquid interface as well as the rate of convective mixing within the bubble trap liquid and heat transfer with the eruption conduit liquid. These issues can be addressed by incorporating a more complete thermodynamic treatment of the complete geyser system, including a model (e.g., relaxation model, Bilicki, and Kestin, 1990; Bilicki et al., 1998) for disequilibrium mass transfer between the vapor and liquid phases. However, this work is beyond the scope of the present paper, and should not affect our principal results governing short-period internal oscillations. We note that some geysers, including Old Faithful (Vandemeuelebrouck et al., 2013) and laboratory analogs (Adelstein et al., 2014), exhibit multi-modal behavior with more than one resonant frequency, and disequilibrium heat and mass transfer between the vapor and liquid phases may explain the longer-period resonances.

The conduit geometry employed in our model is a highly idealized representation of a natural system. In natural systems the conduit geometry is expected to be considerably more complex, with potentially large variations in the conduit cross-sectional areas as a function of depth, and a bubble trap that could be comprised of multiple, inter-connected cavities or permeable zones, as opposed to a single reservoir. While the eruption conduit geometry of some systems has been constrained, we do not yet have detailed constraints on the bubble trap geometry for any system. Constraining the size and shape of bubble traps in natural systems is thus an important objective for future research that would significantly improve our ability to model and understand the origin of oscillations and other geyser behavior. Constraints on bubble trap geometry may come from ground deformation (Rudolph et al. 2012; Vandemeulebrouck et al. 2014), microseismicity (e.g. Cros et al. 2011; Vandemeulebrouck et al. 2013), or downhole exploration (e.g. Hutchinson et al. 1997; Belousov et al. 2013; Muñoz-Saez et al. 2015). We also idealize the fluid filling the conduit and lower region of the bubble trap as being incompressible. A more complete treatment of fluid compressibility in the liquid is beyond the scope of the present study but remains an important goal for future work.

The damping term (Eq. 4) in our equation of motion is subject to considerable uncertainty because there is no closed-form, theoretical expression for viscous dissipation in pipe flow unless the flow is laminar, which is unlikely to be the case in a natural geyser system with rough conduit walls. In principle, the damping coefficient in Eq. 4 could be set to match the amplitude decay rate observed in a natural system, but, as can be seen in the Old Faithful pressure data (Figure 4), it may be difficult to estimate the decay rate in a system that is continually perturbed, and in any case it would be difficult to attribute any physical meaning to the coefficient value given the uncertain nature of the dissipation equation, itself. However, the damping term does not affect the oscillation frequency, so these uncertainties do not affect the ability of the model to fit specific frequencies observed in a data record.

The presence of a bubble trap likely has dynamical consequences beyond the modulation of internal oscillations. Including a bubble trap in a laboratory geyser can lead to multi-modal eruption behavior (Adelstein et al., 2014), and similar effects may occur in natural geysers though our model does not provide a means to study eruption-cycle behavior.

5. CONCLUSIONS

1. Bubble trap geyser configurations generate oscillatory behavior when compressible gas (steam or non-condensable gas) is loaded by liquids in a laterally-offset eruption conduit.
2. The system behaves as a stable, damped oscillator under physically plausible conditions.
3. The resonant period of oscillation is controlled primarily by the size of the eruption conduit (S_c) relative to the size of the bubble trap (S_b) and the relative amounts of gas and liquid in the system, which controls the position of the gas-liquid interface (z_1) in the bubble trap. We

derived a simple mathematical formula to predict the oscillation frequency as a function of the governing parameters.

4. Our model can explain the frequency of the internal oscillations observed for Old Faithful geyser, including the systematic frequency increase observed during the recharge phase, using conduit geometry parameters from the literature.

ACKNOWLEDGMENTS

This work owes a debt of gratitude to a variety of colleagues with whom we have discussed geyser dynamics in the field and lab over the past several years. We are especially grateful for discussions with Shaul Hurwitz, Michael Manga, Jean Vandemeuelebrouck, and Leif Karlstrom. We thank the editor, two anonymous reviewers, and Jean Vandemeulebrouck for their comments.

REFERENCES CITED

Adelstein, E., A. Tran, C. M. Saez, A. Shteinberg, and M. Manga (2014), Geyser preplay and eruption in a laboratory model with a bubble trap, *Journal of Volcanology and Geothermal Research*, *285*(0), 129–135, doi:10.1016/j.jvolgeores.2014.08.005.

Alexandrov, D. V., I. A. Bashkirtseva, and L. B. Ryashko (2016), Analysis of noise-induced eruptions in a geyser model, *Eur. Phys. J. B*, *89*(3), 62, doi:10.1140/epjb/e2016-60982-0.

Anatolyevich, K. D. (2013), Thermo-mechanical Model of Geysers, *International Journal of Mechanic Systems Engineering*, *3*(2), 58–66.

Belousov, A., Belousova, M., and A. Nechayev (2013), Video observations inside conduits of erupting geysers in Kamchatka, Russia, and their geological framework: Implications for the geyser mechanism, *Geology*, 41, 387-390, doi:10.1130/G33366.1.

Bilicki, Z., and J. Kestin (1990), Physical Aspects of the Relaxation Model in Two-Phase Flow, *Proceedings of the Royal Society of London A: Mathematical, Physical and Engineering Sciences*, *428*(1875), 379–397, doi:10.1098/rspa.1990.0040.

Bilicki, Z., D. Kardas, and E. E. Michaelides (1998), Relaxation Models for Wave Phenomena in Liquid-Vapor Bubble Flow in Channels, *J. Fluids Eng*, *120*(2), 369–377, doi:10.1115/1.2820657.

Birch, F., and G. C. Kennedy (1972), Notes on geyser temperatures in Iceland and Yellowstone National Park, *in* Heard, H.C., Borg, I.Y., Carter, N. L., and Raleigh, C. B., eds., Flow and fracture of rocks: Washington, D.C., American Geophysical Union Monograph Series, v. 16, 329-336.

Bunsen, R. W. (1847), Physikalische Beobachtungen uber die hauptsachlichsten Geysir Islands, *Annalen der Physik und Chemie*, 83, p. 159-170.

Cros, E., Roux, P., Vandemeulebrouck, J., and S. Kedar (2011), Locating hydrothermal acoustic sources at Old Faithful Geyser using Matched Field Processing, *Geophysical Journal International*, 187, 385-393, doi:10.1111/j.1365-246X.2011.05147.x.

Dowden, J., P. Kapadia, G. Brown, and H. Rymer (1991), Dynamics of a geyser eruption, *Journal of Geophysical Research*, *96*(B), 18059–18071, doi:10.1029/91JB01584.

Grant, M.A., and M.L. Sorey (1979), The compressibility and hydraulic diffusivity of a water-steam flow, *Water Resources Research*, 15, 684-686, doi:10.1029/WR015i003p00684.

Hutchison, R. A., J. A. Westphal, and S. W. Kieffer (1997), In situ observations of Old Faithful Geyser, *Geology*, 25, 875-878.

Hurwitz, S. and M. Manga (2016), The Fascinating and Complex Dynamics of Geyser Eruptions. *Annual Review of Earth and Planetary Sciences*, *45*(1).

Hurwitz, S., L. E. Clor, R. B. McCleskey, D. K. Nordstrom, A. G. Hunt, and W. C. Evans (2016), Dissolved gases in hydrothermal (phreatic) and geyser eruptions at Yellowstone National Park, USA, *Geology*, *44*(3), 235–238, doi:10.1130/G37478.1.

Ingebritsen, S. E., and S. A. Rojstaczer (1993), Controls on Geyser Periodicity, *Science*, *262*(5135), 889–892, doi:10.1126/science.262.5135.889.

Kagami, H. (2010), An Extended Dynamic Model of a Geyser Induced by an Inflow of Gas (2): Effects of Various Shapes and Repeated Expansions and Contractions in an Underground Watercourse, *Data Science Journal*, IGY110-IGY120.

Karlstrom, L., S. Hurwitz, R. Sohn, J. Vandemeulebrouck, F. Murphy, M. L. Rudolph, M. J. S. Johnston, M. Manga, and R. B. McCleskey (2013), Eruptions at Lone Star Geyser, Yellowstone National Park, USA: 1. Energetics and eruption dynamics: *J. Geophys. Res.*, 118, 4048-4062, doi:10.1002/jgrb.50251.

Kieffer, S. W. (1977), Sound speed in liquid-gas mixtures: water-air and water-steam, *J. Geophys. Res.*, *82*(20), 2895–2904.

Kedar, S., H. Kanamori, and B. Sturtevant (1998), Bubble collapse as the source of tremor at Old Faithful Geyser, *J. Geophys. Res.*, 103, 24,283-24,299.

Kieffer, S. (1984), Seismicity of Old Faithful Geyser: An isolated source of geothermal noise and possible analogue of volcanic seismicity, *Journal of Volcanology and Geothermal Research*, 22, 59-95, doi:10.1016/0377-0273(84)90035-0.

Kieffer, S. W. (1989), Geologic nozzles, *Rev. Geophys.*, *27*(1), 3–38, doi:10.1029/RG027i001p00003.

Mackenzie, G.S. (1811), Travels in the Island of Iceland: Edinburgh, Allam and Company, 27 p.

Muñoz-Saez, C., M. Manga, S. Hurwitz, M. L. Rudolph, A. Namiki, and C-Y Wang, (2015), Dynamics within geyser conduits, and sensitivity to environmental perturbations: Insights from a periodic geyser in the El Tatio geyser field, Atacama Desert, Chile, *Journal of Volcanology and Geothermal Research*, 292, 42-55, doi:10.1016/j.jvolgeores.2015.01.002.

Namiki, A., C. Munoz Saez, and M. Manga (2014), El Cobreloa: A geyser with two distinct eruption styles, *Journal of Geophysical Research (Solid Earth)*, *119*(8), 6229–6248, doi:10.1002/2014JB011009.

O'Hara, K. D., and E. K. Esawi (2013), Model for the eruption of the Old Faithful geyser, Yellowstone National Park, *GSA Today*, *23*, 4–9.

Pedocchi, F., and M. H. Garcia (2009), Friction coefficient for oscillatory flow: the rough–smooth turbulent transition, *Journal of Hydraulic Research*, *47*(4), 438–444, doi:10.1080/00221686.2009.9522019.

Rinehart, J.S. (1980), Geysers and geothermal energy, New York, Springer-Verlag, 223 p.

Rudolph, M. L., M. Manga, S. Hurwitz, M. Johnston, L. Karlstrom, and C.-Y. Wang (2012), Mechanics of Old Faithful Geyser, Calistoga, California, *Geophysical Research Letters*, *39*(24), L24308, doi:10.1029/2012GL054012.

Steinberg, G.S., Merzhanov, A.G., and Steinberg, A.S. (1981), Geyser process: Its theory, modeling, and field experiment, *Modern Geology,* 8, 67-70.

Vandemeulebrouck, J., Roux, P., and E. Cros (2013), The plumbing of Old Faithful Geyser revealed by hydrothermal tremor, *Geophysical Research Letters*, 40, 1989-1993, doi:10.1002/grl.50422.

Vandemeulebrouck, J., Sohn, R.A., Rudolph, M.L., Shurwitz, S., Manga, M., Johnston, M.J.S., Soule, S.A., McPhee, D., Glen, J.M.G., Karlstrom, L., and F. Murphy (2014), Eruptions at Lone Star geyser, Yellowstone National Park, USA: 2. Constraints on subsurface dynamics, *Journal of Geophysical Research*, 119, doi:10.1002/2014JB011526

Wagner, W., Cooper, J. R., Dittmann, A., Kijima, J., Kretzschmar, H.-J., Kruse, A., Mareš, R., Oguchi, K., Sato, H., Stöcker, I., Šifner, O., Takaishi, Y., Tanishita, I., Trübenbach, J., and T. Willkommen, (2000), The IAPWS Industrial Formulation 1997 for the Thermodynamic Properties of Water and Steam, *J. Eng. Gas Turbines & Power*, 122, 150-182.

White, D. (1967), Some principles of geyser activity, mainly from Steamboat Springs, Nevada, *American Journal of Science*, 265, 641-684, doi:10.2475/ajs.265.8.641.

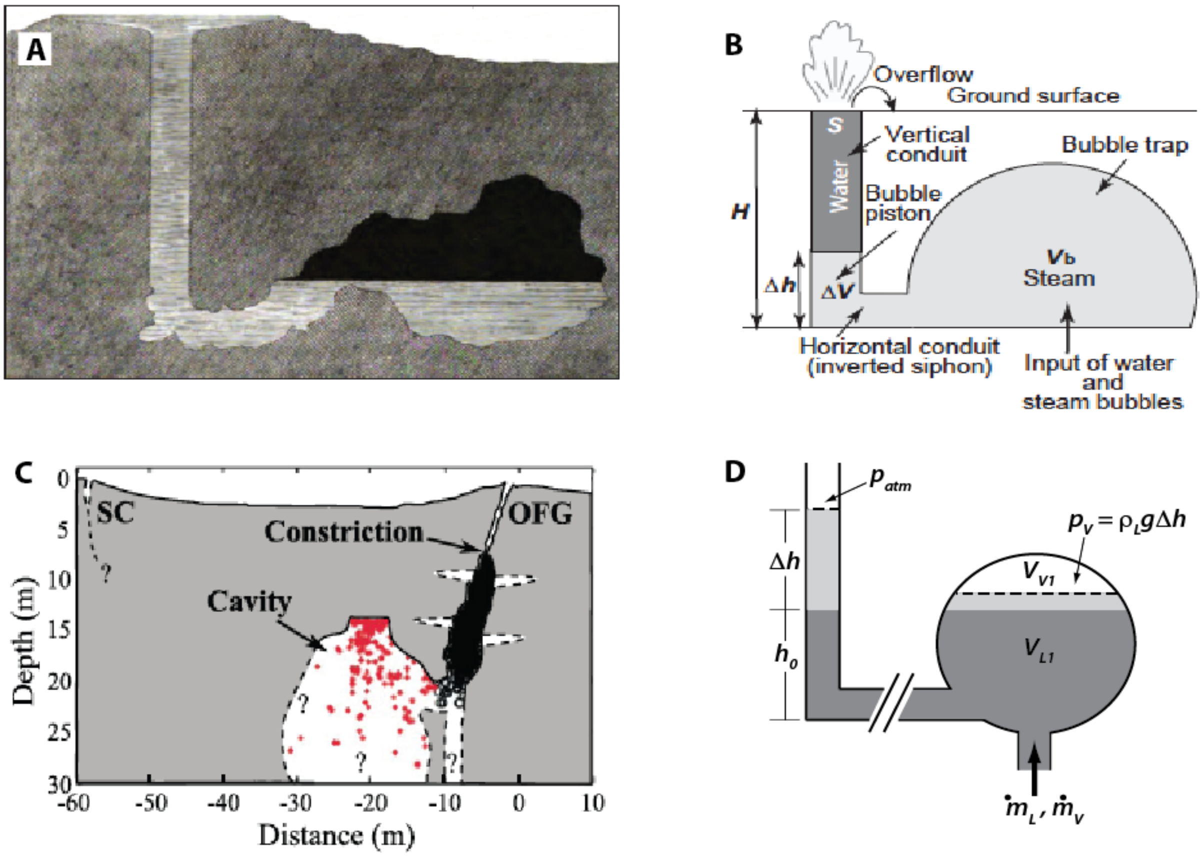

Figure 1: Bubble trap conceptualizations. A) Notional drawing of conduit system underlying the Geysir system in Iceland, from Mackenzie (1811). B) Schematic of conduit systems hypothesized for geysers in Geyser Valley, Kamchatka, Russia, from Belousov et al., 2013. C) Cross-section of conduit system for Old Faithful in Yellowstone National Park, USA, from Vandemeulebrouck et al., (2013). D) Schematic of bubble trap configuration for Lone Star geyser in Yellowstone National Park, USA, from Vandemeulebrouck et al., (2014).

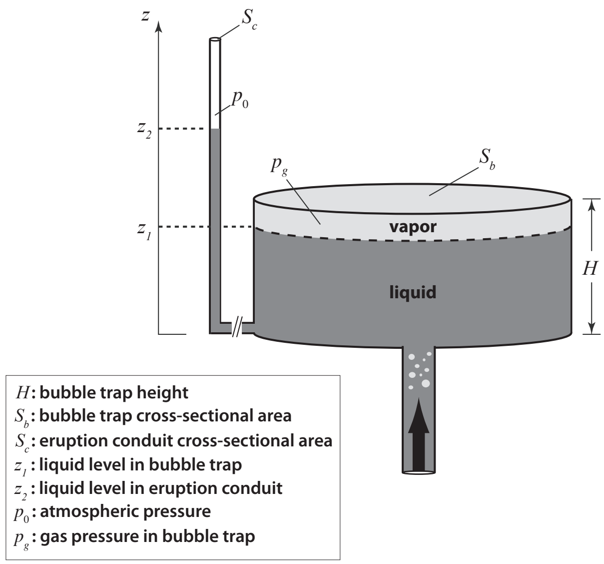

Figure 2: Idealized representation of a bubble trap geyser configuration. Fluid enters the bubble trap and incoming gas is sequestered beneath the roof of a reservoir that is offset from the eruption conduit.

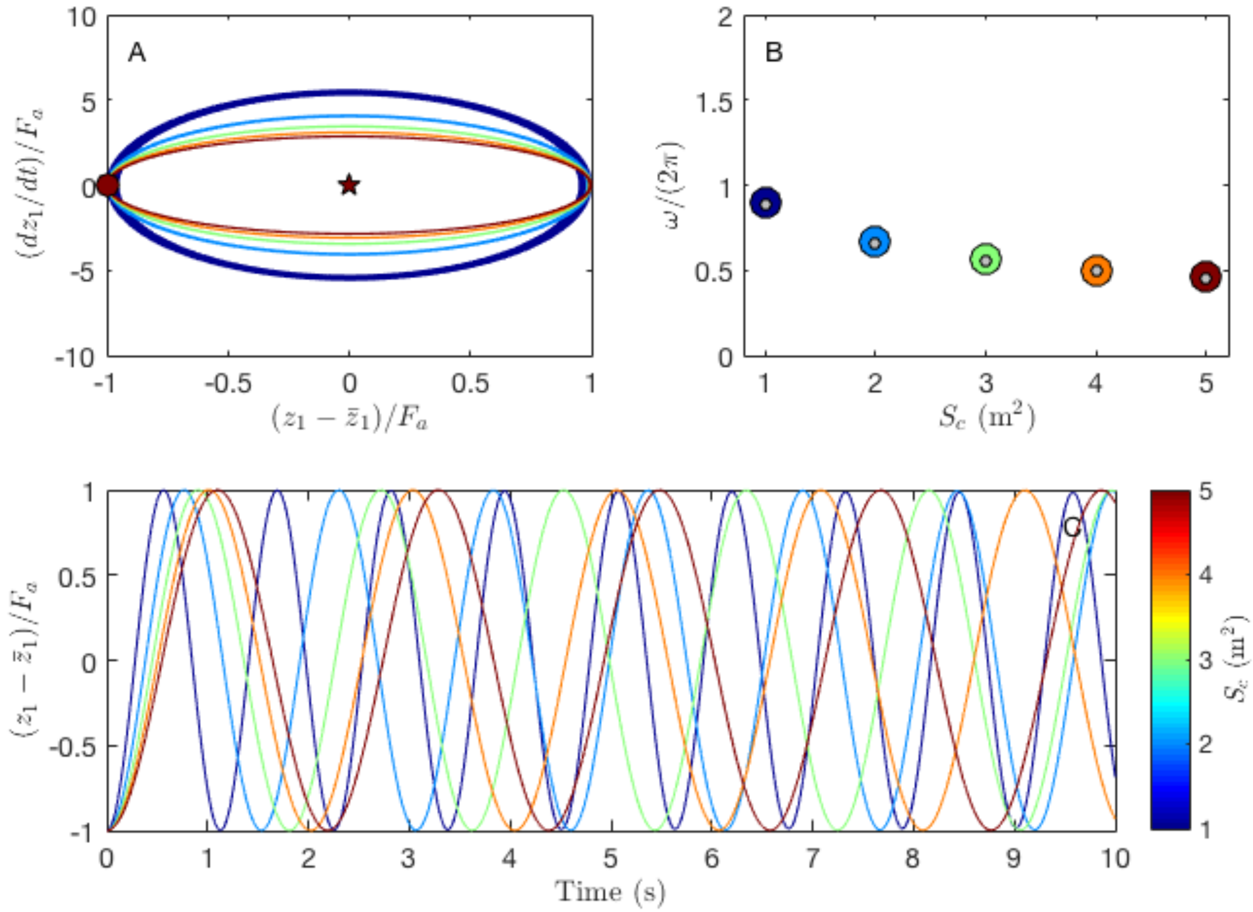

Figure 3: Behavior of Ideal Gas model and sensitivity to parameter choices. Colors correspond to model realizations with different choices of conduit cross-section, S_c. (A) Phase space plot showing perturbation of liquid level (horizontal axis) vs. interface velocity (vertical axis). (B) Dominant frequency of oscillations, from Fourier analysis of numerical experiments (colored circles) and approximate analytic solution (gray dots). (C) Dimensionless displacement of liquid level vs. dimensionless time colors of lines and symbols in all panels correspond to color bar.

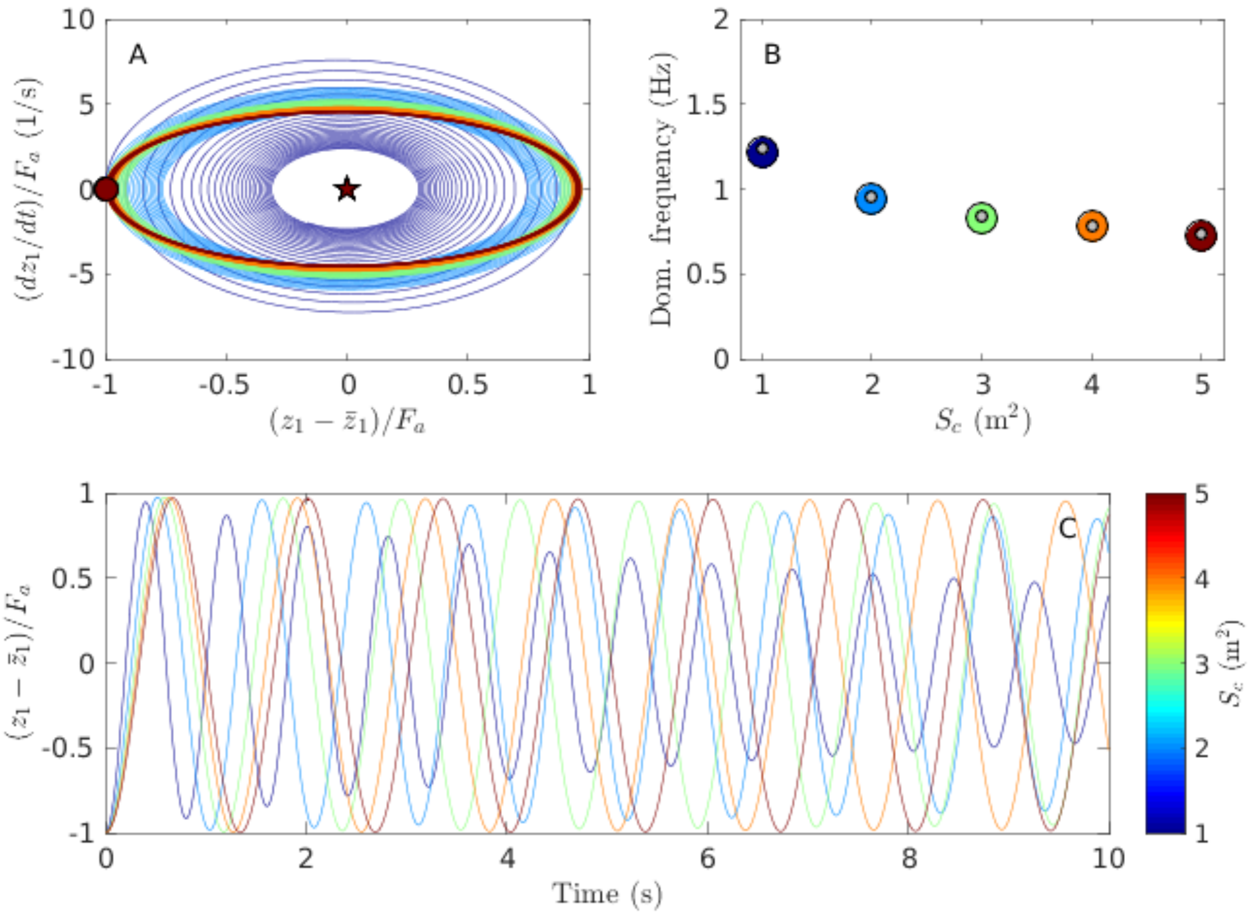

Figure 4: Behavior of steam model and sensitivity to changes in position of vapor-liquid interface in bubble trap ($z_{1,0}$). (A) Phase space behavior. (B) Resonant frequency vs. position of vapor-liquid interface. Colored circles represent Fourier analysis of numerical experiments and gray dots represent approximate analytical solution. (C) Position of vapor-liquid interface vs. time for different values of $z_{1,0}$.

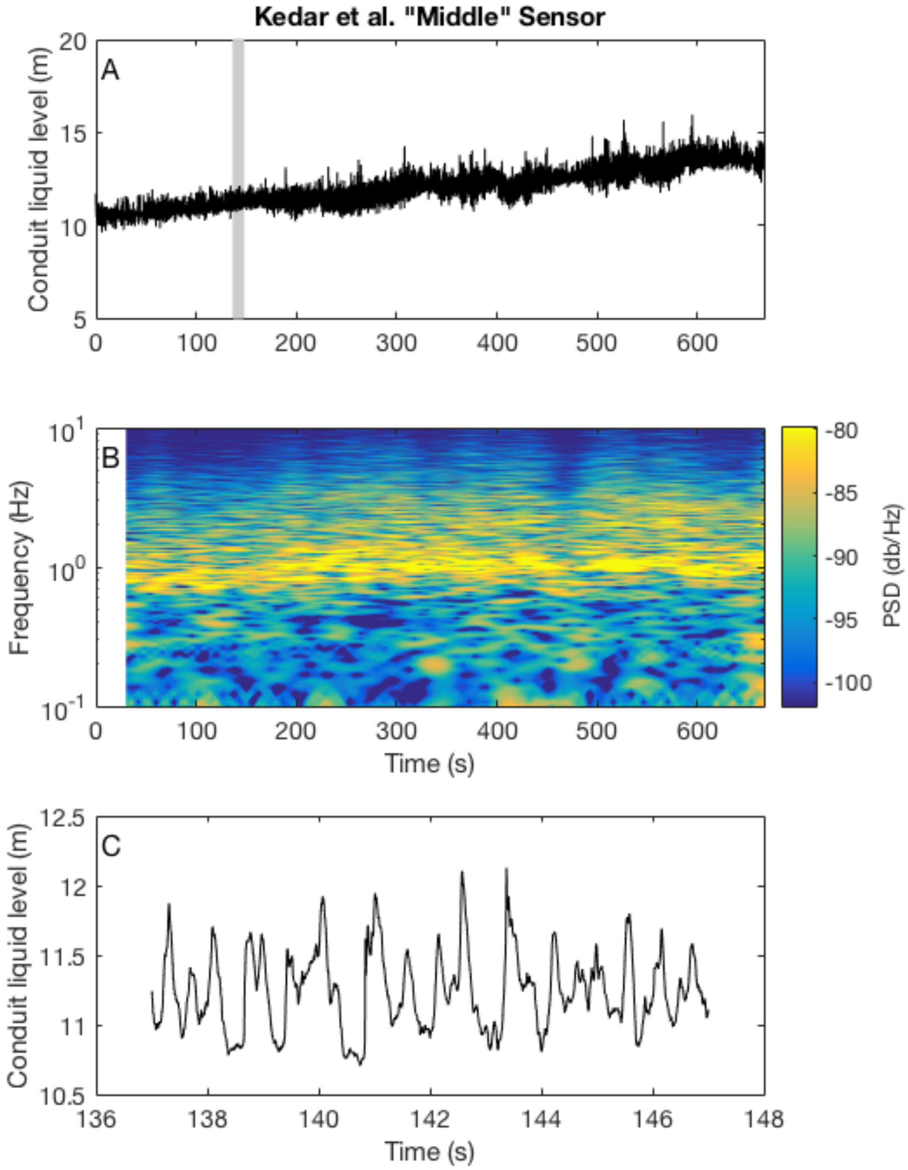

Figure 5. Conduit pressure data from Kedar et al., (1998), obtained during the recharge phase of Old Faithful Geyser. A) Pressure time-series data from the 'middle' sensor, with pressure units converted into water level above the bottom of the conduit. Grey bar shows time period of zoomed-in pressure data shown in panel C. B) Spectrogram of pressure data over same time period as panel A, with yellow colors indicating high-amplitudes and blue colors indicating low-amplitudes. Arrows denote approximate resonant frequencies at the beginning (0.7 Hz) and end (1.0 Hz) of the time window. C) Zoom-in showing 10 s of pressure data from time period indicated by gray bar in panel A showing that the system is perturbed on time-scales shorter than the resonant period, which gives rise to the spectral complexities observed in panel B.

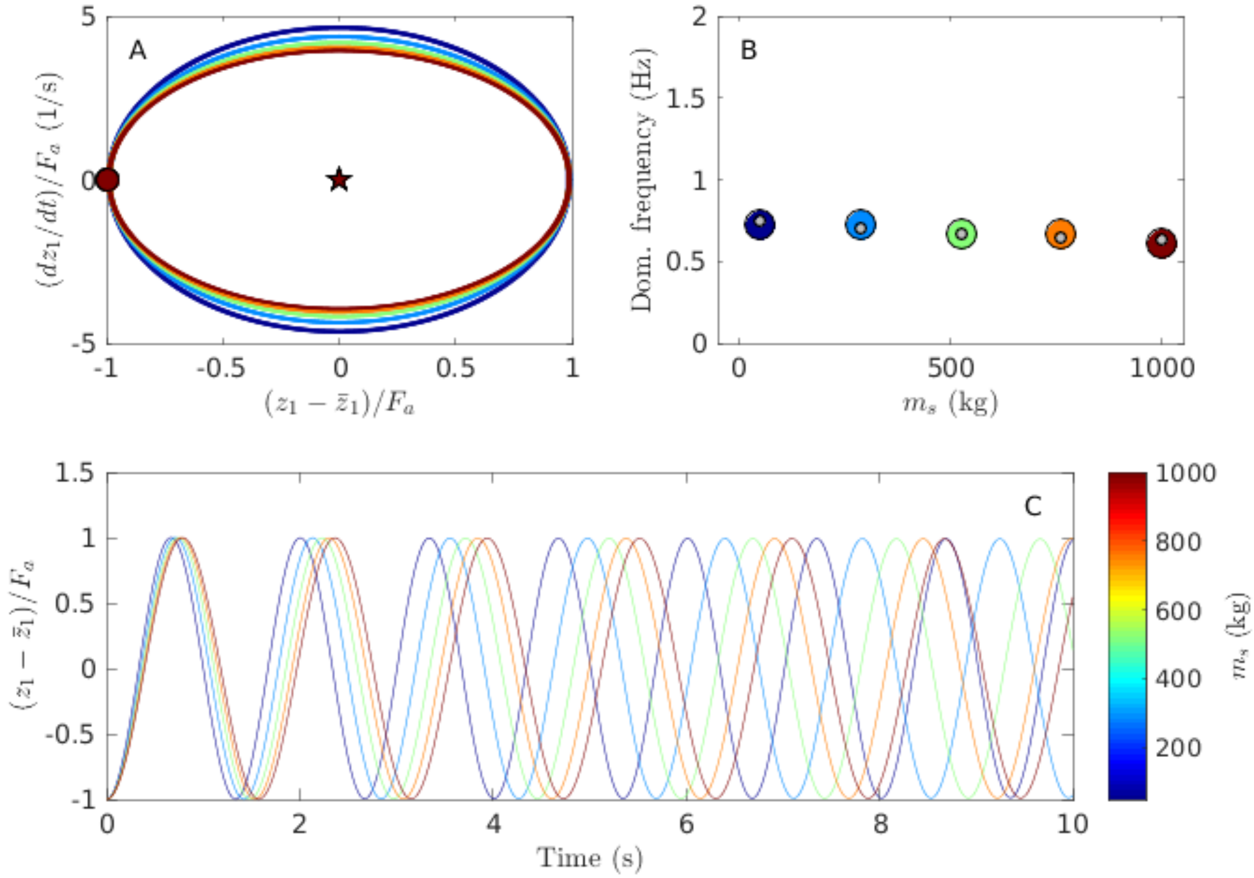

Figure 6: Behavior of the steam model during recharge. Starting from the reference configuration (Table 2), fluid mass is added with twice the initial saturation enthalpy. (A) Phase-space behavior. (B) Relationship between frequency of oscillations and mass added. Colored circles represent Fourier analysis of numerical experiments and gray dots represent approximate analytical solution. (C) Variation of bubble trap liquid level.

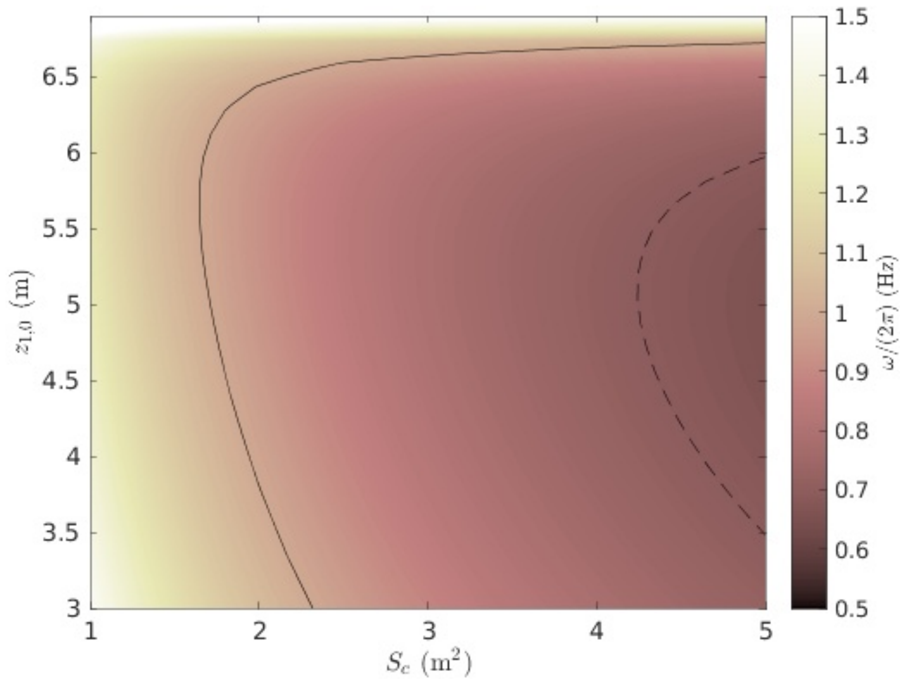

Figure 7: Oscillation frequency tradeoff between vapor-liquid interface position $z_{1,0}$ and conduit cross sectional area (S_c) for the isenthalpic steam model. Contours shown correspond to 0.7 Hz (dashed) and 1.0 Hz (solid).

Symbol, units	Description
g, m/s^2	gravitational acceleration
R, J/mol K	universal gas constant
p_0, Pa	atmospheric pressure
ρ, kg/m^3	liquid density
V_l, m^3	system liquid volume
p_g, Pa	gas pressure
T, K	gas temperature
n, moles	number of gas moles
H, m	height of bubble trap roof above connector
S_b, m^2	bubble trap cross-sectional area
S_c, m^2	eruption conduit cross-sectional area
C, m	maximum value of z_2
F_s, N	surface tension at gas-liquid interface (assumed zero)
z_1, m	height of gas-liquid interface above connector
z_2, m	height of eruption conduit liquid level above connector
V_g, m^3	system gas volume
t, s	time
F_i, N	inertial force of liquid mass
F_h, N	hydrostatic force
F_f, N	viscous dissipation (frictional) force

Table 1. List of symbols used, with SI units and description.

Dimensional Parameters	
H	7 m
S_b	80 m^2
S_c	5 m^2
T	373 K
P_0	10^5 Pa
g	10 m s^{-2}
ρ	1000 kg m^{-3}

Table 2: Parameter values for OFG-like reference configuration.